Chapter 16
Patient-Specific Surgery Planning for the Fontan Procedure

Christopher M. Haggerty, Lucia Mirabella, Maria Restrepo, Diane A. de Zélicourt, Jarek Rossignac, Fotis Sotiropoulos, Thomas L. Spray, Kirk R. Kanter, Mark A. Fogel, and Ajit P. Yoganathan

Abstract For children born with single ventricle heart defects, the Fontan procedure (right heart bypass via connection of caval veins to pulmonary arteries) is the palliative procedure of choice. Previous research has demonstrated strong coupling

C.M. Haggerty · L. Mirabella · M. Restrepo · D.A. de Zélicourt · A.P. Yoganathan (✉)
Wallace H. Coulter School of Biomedical Engineering, Georgia Institute of Technology and Emory University, Atlanta, GA, USA
e-mail: ajit.yoganathan@bme.gatech.edu

C.M. Haggerty
e-mail: chaggerty3@gatech.edu

L. Mirabella
e-mail: lmirabella3@mail.gatech.edu

M. Restrepo
e-mail: mrestrepo3@gatech.edu

D.A. de Zélicourt
e-mail: diane.dezelicourt@gmail.com

J. Rossignac
College of Computing, Georgia Institute of Technology, Atlanta, GA, USA
e-mail: jarek@cc.gatech.edu

F. Sotiropoulos
Department of Civil Engineering, University of Minnesota, Minneapolis, MN, USA
e-mail: fotis@umn.edu

T.L. Spray · M.A. Fogel
Children's Hospital of Philadelphia, Philadelphia, PA, USA

T.L. Spray
e-mail: spray@email.chop.edu

M.A. Fogel
e-mail: fogel@email.chop.edu

K.R. Kanter
Children's Healthcare of Atlanta, Atlanta, GA, USA
e-mail: kkanter@emory.edu

G.A. Holzapfel, E. Kuhl (eds.), *Computer Models in Biomechanics*,
DOI 10.1007/978-94-007-5464-5_16,

between the geometric characteristics of the surgical construct and the resulting patient-specific hemodynamics, which may relate to the numerous chronic morbidities seen in these patients. The combination of medical imaging, computer graphics and computational fluid simulations has introduced a powerful new paradigm for these procedures: providing the means to model the various options and evaluate the resulting characteristics. This paper details these methodologies, their application to planning interventions, and their contributions to generalizable knowledge of Fontan hemodynamics.

16.1 Introduction

Single ventricle congenital heart defects are lethal if left untreated. The most common surgical intervention, known as the Fontan procedure, creates a right heart bypass by routing systemic venous return to the pulmonary arteries (Fontan and Baudet, 1971), creating the total cavopulmonary connection (TCPC) (de Leval et al., 1988). Despite acceptable operative outcomes, significant long-term complications are common, owing in part to the altered hemodynamics associated with Fontan physiology (Mair et al., 2001). Such complications include arrhythmias, ventricular dysfunction, exercise intolerance, protein-losing enteropathy, and pulmonary arteriovenous malformations (PAVM) (Gersony and Gersony, 2003).

Since its introduction, the TCPC has been the focus of large body of research in an effort to understand how the geometric characteristics of the surgical construct impact the hemodynamics within the connection (de Leval et al., 1996; Sharma et al., 1996; Migliavacca et al., 2003; de Zélicourt et al., 2005). With only one ventricle providing the driving pressure for both the systemic and pulmonary circulations, the general motivation and hypothesis behind such studies are that minimizing the hemodynamic power loss across the connection will provide long-term benefits for cardiovascular health. While many early studies relied on relatively simple models of idealized geometries, the current state-of-the-art employs patient-specific data for both the anatomic and physiologic boundary conditions for computational fluid solvers.

Through such advances, in conjunction with progress in computer science and free-form shape editing, it is now possible to both design and evaluate patient-specific TCPC models (Pekkan et al., 2008). In other words, these engineering tools can be used for prospective surgical planning by modeling any number of possible anatomic variations and characterizing their associated hemodynamics. The applications of such methods extend equally well to either a patient's initial Fontan procedure or, as shown by Sundareswaran et al. (2009a) and de Zélicourt et al. (2011), any subsequent surgical revisions, perhaps necessitated by deteriorating physiology (i.e., Fontan failure). As such, these techniques represent a powerful new paradigm for the approach to Fontan surgery and cardiothoracic surgery as a whole. The objective of this work is to detail the underlying methods and techniques upon which surgical planning builds. Different examples of each method are provided throughout to demonstrate their utility.

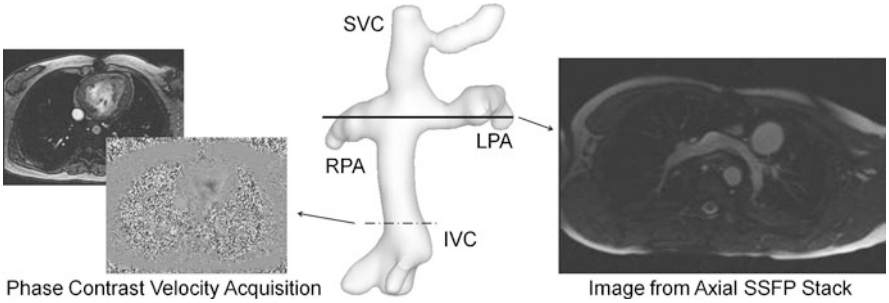

Fig. 16.1 Examples of typically acquired CMR images in relation to a patient-specific TCPC reconstruction (*central panel*). *Left*: magnitude and phase velocity images through the IVC. *Right*: axial steady-state free precession (SSFP) anatomic image through the right and left pulmonary arteries (RPA, LPA); SVC: superior vena cava

16.2 Methods and Results

The fundamental components of the current surgical planning procedure are the following: (i) cardiovascular magnetic resonance (CMR) image acquisition and reconstruction; (ii) virtual surgery, (iii) computational fluid dynamic (CFD) simulations.

16.2.1 CMR Imaging and Image Processing

Medical imaging provides the patient-specific anatomy and boundary conditions that inform the rest of the modeling. CMR is the preferred modality as it provides the means to both image the anatomic structures and make quantitative measurements of blood flow through variations in the sequence of magnetic field excitation. Figure 16.1 shows examples of these various image types in the context of the TCPC. The right image is taken from an axial stack of steady-state free precession images spanning the thorax. Here, the blood pool in the vessels produces a signal (without the use of a contrast agent), facilitating anatomical reconstruction (Frakes et al., 2005). The left set of images shows an instantaneous through-plane phase contrast measurement in a slice through the inferior vena cava (IVC). By acquiring such 2D images through each of the TCPC vessels, the local velocity fields (inlet/outlet boundary conditions) can be measured (Sundareswaran et al., 2009b).

These acquisitions provide the minimum information required to perform the subsequent anatomic and fluid mechanical modeling; however, advances in CMR sequence designs and image processing have provided additional means to directly assess *in vivo* flow patterns (Sundareswaran et al., 2012). Specifically, phase contrast sequences can be expanded to acquire three orthogonal components of the velocity vectors on a single slice; furthermore, the vector values between the slices can be interpolated using a novel divergence-free scheme. Therefore, a stack of such images spanning the TCPC can provide detailed 4D hemodynamic information throughout

the entire volume. As indicated by the recent work of Sundareswaran et al. (2012), these methods of 4D *in vivo* flow visualization and quantification have significant clinical potential. When acquired and analyzed over a larger series of patients, the results can be used to provide insights on a more generalizable level, such as the hemodynamic implications of different approaches to Fontan surgery (extra- vs. intra-cardiac) or the accuracy of computational fluid solvers for analyzing the same flow conditions. The increased availability of these 4D flow imaging sequences, and the development of volumetric phase contrast techniques (Markl et al., 2011), will make such analyses possible on a much broader scale in the near future.

Furthermore, for failing patients referred for surgical planning, these imaging techniques can be an invaluable means to directly identify adverse hemodynamic characteristics, as demonstrated in the following case study.

16.2.1.1 Patient-Specific Case Study

This was an eleven year old patient with bilateral superior vena cavae (SVC), interrupted IVC and azygos vein continuation, and a previous Fontan connection. In this rare and complex anatomy, the majority of inferior venous blood flow is carried by an enlarged azygos vein, which connects to one of the two SVCs. The Fontan baffle therefore carries only hepatic blood from the liver to the pulmonary arteries. Hemodynamic analysis was necessitated by the presence of PAVM in the right lung: arterial to venous shunts within the pulmonary vasculature that bypass the oxygenating alveolar beds, leading to progressive hypoxia. Studies suggest that this condition can develop because of a lack of hepatic blood flow, and a so-called 'hepatic factor', to either or both lungs (Duncan and Desai, 2003). This strong and well-characterized relationship between PAVM and the local TCPC hemodynamics has made it the primary indication in the preliminary series ($n = 15$) of patient-specific surgical planning; identifying connection designs that achieve a balanced hepatic flow distribution (HFD) has been shown to be effective in alleviating the disease state. Therefore, the objective of the analysis was to (i) confirm the unilateral distribution of hepatic flow from the liver, which is consistent with PAVM in the right lung; (ii) determine the factors mediating such undesirable hemodynamics.

Figure 16.2 (left panel) provides a single slice example of the coronal 4D MRI data acquired: the magnitude image is shown on top and the three orthogonal vector components (anatomically: anterior-posterior, foot-head, left-right) are shown at the bottom. The results from the volumetric interpolation are also shown (right panel) as instantaneous velocity streamlines, shaded based on the vessel of origin (LSVC flow omitted). The overlaid numbers report the time-averaged contribution of each vessel to the total flow, as determined from analysis of the through-plane phase contrast data.

From the reconstructed velocity field, it was appreciated that flow through the left-sided hepatic venous baffle (HepV; blue streamlines) was both very low in magnitude and heavily influenced by the momentum of the RSVC and Azygos (Azy)

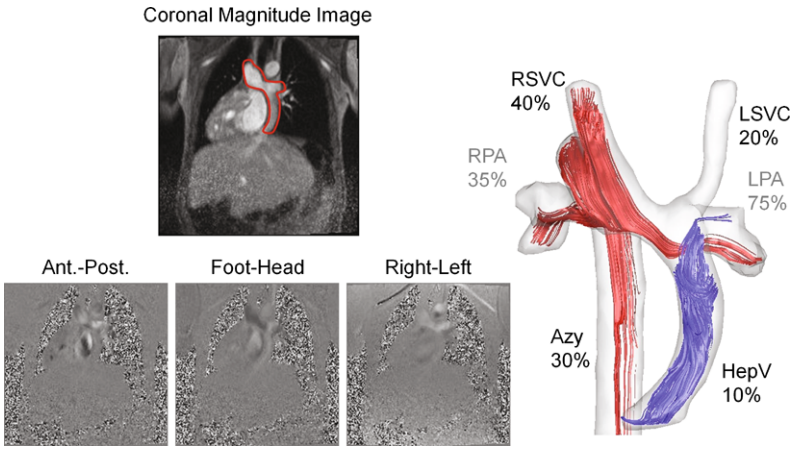

Fig. 16.2 *Left panel*: magnitude (*top*) and 3D phase contrast velocity (*bottom*) images for a single slice and cardiac phase from the coronal stack acquired. The TCPC is outlined in the magnitude image for reference. *Right panel*: TCPC reconstruction with instantaneous velocity streamlines from the 4D interpolation. Overlaid numbers represent time-averaged percentage contribution for each vessel to the total venous return. Azy-Azygos vein; HepV-Hepatic venous baffle

flows (red streamlines), which comprised 70 % of the total volume flow rate. Furthermore, only 35 % of flow through the connection exited the RPA, meaning that a significant portion of the RSVC + Azy flow had to traverse the connection to exit the LPA. This analysis is consistent with the right-to-left path of some of the red streamlines seen in Fig. 16.2, which influenced the hepatic streamlines and forced a unilateral (left) hepatic distribution, consistent with right-sided PAVM. Based on these observations, which were made possible by the ability to visualize the *in vivo* flow structures, it is evident that a successful surgical revision of this connection to address the PAVM must overcome: low momentum hepatic flow, high momentum superior venous flows, and potentially unfavorable results of their direct interaction.

16.2.2 Virtual Surgery

The use of CMR anatomical data to produce patient-specific models for detailed computational and/or experimental analyses has been a standard practice for the past decade (Frakes et al., 2003; de Zélicourt et al., 2005). However, such techniques can only measure and characterize the current physiology; to prospectively create connections in a realistic way to explore 'what if' scenarios required additional developments from the field of computer vision. To this end, a virtual interface was developed that allowed the user to import patient-specific anatomical reconstructions (e.g., the TCPC, single ventricle and atria, aorta, pulmonary veins) and mimic surgical gestures in the placement and deformation of the IVC baffle using free-form haptic devices (Pekkan et al., 2008). Thus, for a given patient anatomy: the size and

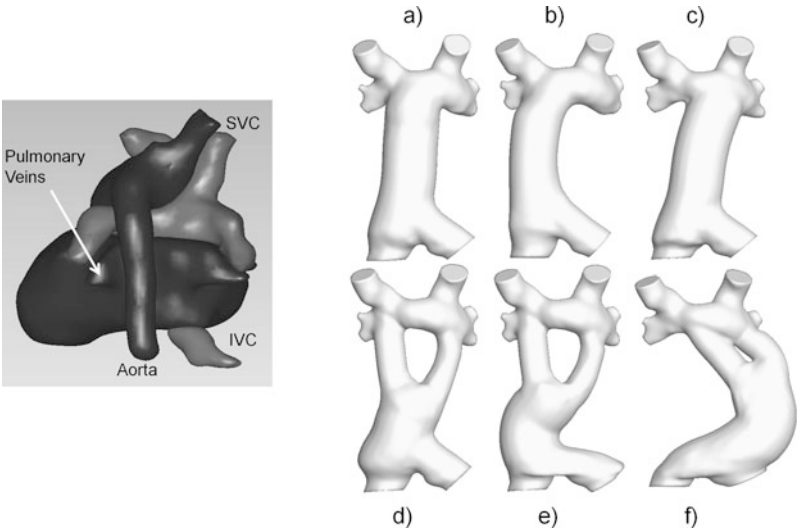

Fig. 16.3 *Left panel*: example of reconstructed TCPC and surrounding anatomy to be imported into virtual surgery interface for simulation of Fontan completion (IVC baffle to PA). *Right panel*: virtual options designed for a patient with bilateral SVCs and distinct atrial connections for the IVC and hepatic vein. Variations in IVC connection type (single baffle vs. Y-graft), baffle offset with respect to the PAs, and means of unifying IVC and hepatic flows are demonstrated

shape of the PAs, the orientation of the SVC-PA junction, and the size and location of surrounding anatomical structures, all potential options for the size and placement of the IVC baffle can be explored and generated in advance of the surgical procedure.

Figure 16.3 (left side) shows an example of the patient-specific reconstructions that are frequently incorporated into the virtual surgery interface. It is critical that surrounding structures, not simply the TCPC vessels, be included so as to visually provide the constraints and the relevant landmarks that surgeons rely on in the operating room. Otherwise, designing the connection 'in a vacuum' may yield unrealistic results. The right side of Fig. 16.3 provides a series of connections designed for a single patient with bilateral SVCs and separate IVC and hepatic connections to the atrium (prior to Fontan completion). These images serve to both demonstrate the capabilities of the software and emphasize its utility. In such complex anatomical configurations, it is possible to parametrically vary connection approach (top row vs. bottom row), baffle placement (a vs. b vs. c) or angle, and other patient-specific considerations: in this case, the means of joining the hepatic and IVC flows (a–d vs. e–f). Given that the examples shown are all reasonable approximations of the way in which any given surgeon might approach the connection of such a patient, the ability to both identify such options and, as detailed in the follow section, characterize the hemodynamic consequences a priori is a valuable asset.

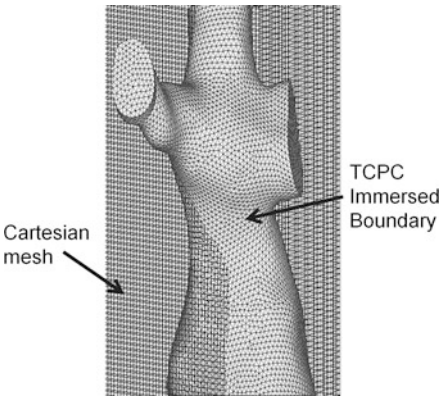

Fig. 16.4 Registration of TCPC surface mesh (*light gray*) within regular, background Cartesian grid

16.2.3 Computational Fluid Dynamics

The final critical component of the surgical planning tool set is the means to predict hemodynamic outcomes for all virtually designed connection options. For this, computational fluid dynamics (CFD) solvers play a central role. The subsequent sections provide descriptions of the important considerations inherent to such modeling, followed by selected results from preliminary experiences.

16.2.3.1 Solver Description

It is important to note that any validated computational fluid solver can be used to yield the needed results for these analyses; however, the program presently described has the advantage of simplifying the process of generating the discretized computational mesh. In cases where there are a large number of possible anatomic solutions to evaluate, this advantage is non-trivial.

The solver is based on the sharp-interface immersed boundary approach of Gilmanov and Sotiropoulos (2005). This method, rather than requiring a dense, high quality mesh of volume elements throughout the computational domain, only requires the boundary (i.e., the walls of the TCPC) to be discretized with two-dimensional triangular elements. This surface is then immersed and registered within a regular Cartesian grid (Fig. 16.4) to be segregated into fluid nodes (those falling within the boundaries), 'immersed boundary' (IB) nodes (nodes within the boundaries but immediately adjacent to the sharp-interface of the wall), and wall nodes (those external to the boundary). The 3D, unsteady incompressible Navier-Stokes equations must then only be solved on the internal fluid nodes (discretized in a hybrid staggered/non-staggered layout), with the wall boundary conditions (typically, the no-slip condition), imposed iteratively on the IB nodes. As described by de Zélicourt et al. (2009) this method is further simplified by recasting the problem into an unstructured Cartesian grid to reduced the required memory overhead of the discarded wall nodes.

16.2.3.2 Boundary Conditions

From the CMR analysis, specifically the through-plane phase contrast images, time-varying flow conditions across the cardiac cycle are known for all TCPC vessels of interest. The standard practice of TCPC simulations with this IB solver is to impose these flows (either as time-averaged or time-varying flat velocity profiles) at the inlets and the prescribed flow split at the outlets of the computational domain. Surgical modeling simulations present the additional challenge of physiologic changes (perhaps both acute and chronic) in the rest of the circulatory system in response to Fontan surgery. The work of Fogel et al. (1996) indicates that such changes have an impact on the cardiac output and thus systemic venous flows; the impact on the pulmonary vasculature and/or distribution has only be reported in a single patient case (Pennati et al., 2011) demonstrating unanticipated variations. In other words, simply imposing the measured flow conditions on the surgical model is unlikely to sufficiently represent the post-operative state.

There are thus several strategies that have been employed to combat this challenge. First is the parametric variation of the outflow distributions imposed: if a 60 %/40 % RPA/LPA distribution was measured pre-operatively, the proposed options might also be evaluated at 40/60, 50/50, and 70/30 to simulate possible outflow distributions. The finite and physiologically bounded nature of this parameter space facilitates these variations. The primary guide in making such determinations is the presence and hypothesized evolution of PAVMs in the given patient. For example, a presumed decrease in the number of malformations present would increase the effective vascular resistance of the pulmonary beds, leading to a decrease in local flow. Additionally, natural growth and development is likely to vary the relative distribution of pulmonary flows over the life of the patient, so identifying solutions that are robustly able to handle such variation is desirable.

Similarly, the inflow conditions can be selectively varied, both with respect to bulk flow rates and relative vessel distributions. However, it is important to note that the parameter space for the inlet values may not be as well constrained as the outlets, both with respect to magnitude and distribution variations, particularly as the number of inlet vessels increases (such as cases like in Fig. 16.2). Furthermore, the factors that mediate such changes, either at the level of the ventricular output or the relative compliances of the systemic vascular bed, are not as easy to define or predict, and no data yet exist in the literature to set a precedent.

Significant research and ongoing development efforts are focused on the use of multi-dimensional models to create a comprehensive view of the cardiovascular circuit (Laganà et al., 2005; Migliavacca et al., 2006; Kim et al., 2009). That is, the three-dimensional CFD domain is coupled with 0-dimensional lumped parameter models to capture the global hemodynamics. This multi-dimensional approach may address some of the limitations of prospective modeling efforts by providing a more rigorous means of determining the post-operative boundary conditions, particularly for the inlets. Of course, validation of such models will be critical and, as the work of Pennati et al. (2011) demonstrates, lumped parameter models alone may not be sufficient for capturing the range of possible patient-specific responses.

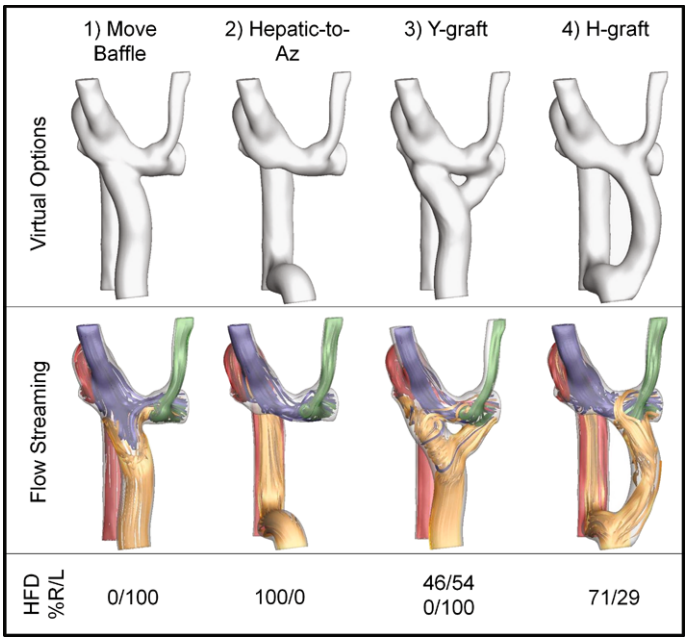

Fig. 16.5 *Top row*: a subset of the surgical models created for a failing patient with right lung PAVM. *Middle row*: flow streaming results (hepatic flow represented by gold streamlines) under equal pulmonary outflow conditions. *Bottom row*: quantitative flow distribution results as a percentage of hepatic flow exiting the right (R) or left (L) pulmonary artery. For option 3, the results of two possible variations on the same topology are shown

16.2.3.3 Patient-Specific Case Study

Returning to the patient case detailed in Sect. 16.2.1.1, Fig. 16.5 details a subset of the virtual surgical options created and their associated flow streaming results. The investigated options were intended to assess the impact of: (i) repositioning the hepatic baffle (option 1); (ii) merging the hepatic flow with another vessel to promote mixing (option 2); or (iii) bifurcating the hepatic flow laterally to either side of the connection (options 3 and 4). The gold streamlines in the middle row of Fig. 16.5 show the hepatic flow streaming results for each of these options with the quantitative results shown in the bottom row in terms of the percentage of hepatic flow perfusing the right or left pulmonary artery.

The results reveal substantial sensitivity of the flow streaming characteristics to the surgical baffle placement, underscoring both the significant challenge in surgically treating this particular patient, as well as the tremendous value of this modeling work in providing such information to the clinician. For option 1, simply repositioning the hepatic baffle closer to the RPA was shown to provide no benefit to hepatic-RPA flow because of the relative dominance of the RSVC and Azygos flows (blue streamlines seen impinging into the hepatic baffle). On the other hand, option 2 reached the opposite extreme in that all hepatic flow went to the RPA (by way of

the azygos vein). While this outcome would be acutely positive in addressing the right-sided PAVM, it is not a desirable long-term result as it presents a risk of future left lung PAVM development. Two different HFD values are provided for option 3 because multiple Y-graft designs were created and evaluated, with the right branch of the bifurcation being positioned slightly further to the right in one case (46 %) than the other (0 %). This drastic difference in potential outcome made such an approach undesirable given the uncertainty in how precisely the surgeon can mimic the virtual model in the operating room (i.e., the option was not robust with respect to the exact detail of surgical implementation). Finally, option 4 took an alternative approach to flow bifurcation by routing the right branch to the azygos vein (similar to option 2) while maintaining the original hepatic connection to provide flow to the left lung. Of the options tested, this design was predicted to yield the best outcome (71 % HFD to the RPA with a 50/50 outflow split of the total flow imposed as the boundary condition), presumably because it was successfully able to avoid direct competition between the low momentum hepatic flow and high momentum SVC/azygos flows. This 'H-graft' connection was ultimately selected for surgical implementation and, although no post-operative image data are available, arterial oxygen saturations were clinically seen to improve from 70 to 87 % four months post-operatively, which is indicative of regression of the PAVM, as predicted.

16.3 Conclusions

Through multi-disciplinary research collaborations and technological developments, image-based computational surgery planning for the Fontan procedure has become a reality. This ability greatly increases the resources available to clinicians in patient-specific decision making by supplementing intuition and experience with modeled predictions tailored to the specific case and intervention of interest. Obviously, these techniques have potential to extend far beyond Fontan surgery into the broader realm of cardiovascular procedures, but to do so requires a similar understanding of the specific hemodynamic end points that mediate the desired clinical outcome (as HFD relates to PAVM). Furthermore, surgical planning for the Fontan is still in its preliminary stages and much work remains to be done, perhaps most importantly, developing and validating the means of predicting what the post-operative boundary conditions will be. Nevertheless, the novelty and value of these techniques in translating engineering principles into actionable clinical tools are clear and the present an exciting new paradigm for cardiothoracic modeling and interventions.

Acknowledgements This work was supported by the National Heart, Lung, and Blood Institute through Grants HL67622 and HL098252, and through American Heart Association Pre-Doctoral Fellowships.

References

de Leval MR, Kilner P, Gewillig M, Bull C (1988) Total cavopulmonary connection: a logical alternative to atriopulmonary connection for complex Fontan operations. Experimental studies and early clinical experience. J Thorac Cardiovasc Surg 96:682–695

de Leval MR, Dubini G, Migliavacca F, Jalali H, Camporini G, Redington A, Pietrabissa R (1996) Use of computational fluid dynamics in the design of surgical procedures: application to the study of competitive flows in cavopulmonary connections. J Thorac Cardiovasc Surg 111:502–513

de Zélicourt DA, Pekkan K, Wills L, Kanter KR, Forbess J, Sharma S, Fogel MA, Yoganathan AP (2005) In vitro flow analysis of a patient-specific intraatrial total cavopulmonary connection. Ann Thorac Surg 79:2094–2102

de Zélicourt DA, Ge L, Wang C, Sotiropoulos F, Gilmanov A, Yoganathan AP (2009) Flow simulations in arbitrarily complex cardiovascular anatomies—an unstructured Cartesian grid approach. Comput & Fluids 38:1749–1762

de Zélicourt DA, Haggerty CM, Sundareswaran KS, Whited BS, Rossignac JR, Kanter KR, Gaynor JW, Spray TL, Sotiropoulos F, Fogel MA, Yoganathan AP (2011) Individualized computer-based surgical planning to address pulmonary arteriovenous malformations in patients with a single ventricle with an interrupted inferior vena cava and azygous continuation. J Thorac Cardiovasc Surg 141:1170–1177

Duncan BW, Desai S (2003) Pulmonary arteriovenous malformations after cavopulmonary anastomosis. Ann Thorac Surg 76:1759–1766

Fogel MA, Weinberg PM, Chin AJ, Fellows KE, Hoffman EA (1996) Late ventricular geometry and performance changes of functional single ventricle throughout staged Fontan reconstruction assessed by magnetic resonance imaging. J Am Coll Cardiol 28:212–221

Fontan F, Baudet E (1971) Surgical repair of tricuspid atresia. Thorax 26:240–248

Frakes DH, Conrad CP, Healy TM, Monaco JW, Fogel MA, Sharma S, Smith MJ, Yoganathan AP (2003) Application of an adaptive control grid interpolation technique to morphological vascular reconstruction. IEEE Trans Biomed Eng 50:197–206

Frakes DH, Smith MJ, Parks WJ, Sharma S, Fogel MA, Yoganathan AP (2005) New techniques for the reconstruction of complex vascular anatomies from MRI images. J Cardiovasc Magn Reson 7:425–432

Gersony DR, Gersony WM (2003) Management of the postoperative Fontan patient. Prog Ped Cardiol 17:73–79

Gilmanov A, Sotiropoulos F (2005) A hybrid Cartesian/immersed boundary method for simulating flows with 3D, geometrically complex, moving bodies. J Comput Phys 207:457–492

Kim HJ, Vignon-Clementel IE, Figueroa CA, LaDisa JF, Jansen KE, Feinstein JA, Taylor CA (2009) On coupling a lumped parameter heart model and a three-dimensional finite element aorta model. Ann Biomed Eng 37:2153–2169

Laganà K, Balossino R, Migliavacca F, Pennati G, Bove EL, de Leval MR, Dubini G (2005) Multiscale modeling of the cardiovascular system: application to the study of pulmonary and coronary perfusions in the univentricular circulation. J Biomech 38:1129–1141

Mair DD, Puga FJ, Danielson GK (2001) The Fontan procedure for tricuspid atresia: early and late results of a 25-year experience with 216 patients. J Am Coll Cardiol 37:933–939

Markl M, Geiger J, Kilner PJ, Foll D, Stiller B, Beyersdorf F, Arnold R, Frydrychowicz A (2011) Time-resolved three-dimensional magnetic resonance velocity mapping of cardiovascular flow paths in volunteers and patients with Fontan circulation. Eur J Cardiothorac Surg 39:206–212

Migliavacca F, Dubini G, Bove E, de Leval MR (2003) Computational fluid dynamics simulations in realistic 3-D geometries of the total cavopulmonary anastomosis: the influence of the inferior caval anastomosis. J Biomech Eng 125:803–813

Migliavacca F, Balossino R, Pennati G, Dubini G, Hsia TY, de Leval MR, Bove E (2006) Multiscale modelling in biofluidynamics: application to reconstructive paediatric cardiac surgery. J Biomech 39:1010–1020

Pekkan K, Whited B, Kanter KR, Sharma S, de Zélicourt DA, Sundareswaran KS, Frakes DH, Rossignac J, Yoganathan AP (2008) Patient-specific surgical planning and hemodynamic computational fluid dynamics optimization through free-form haptic anatomy editing tool (SURGEM). Med Biol Eng Comput 46:1139–1152

Pennati G, Corsini C, Cosentino D, Hsia TY, Luisi VS, Dubini G, Migliavacca F (2011) Boundary conditions of patient-specific fluid dynamics modelling of cavopulmonary connections: possible adaptation of pulmonary resistances is a critical issue for virtual surgical planning. Interface Focus 1:297–307

Sharma S, Goudy S, Walker P, Panchal S, Ensley A, Kanter KR, Tam V, Fyfe D, Yoganathan AP (1996) In vitro flow experiments for determination of optimal geometry of total cavopulmonary connection for surgical repair of children with functional single ventricle. J Am Coll Cardiol 27:1264–1269

Sundareswaran KS, de Zélicourt DA, Sharma S, Kanter KR, Spray TL, Rossignac J, Sotiropoulos F, Fogel MA, Yoganathan AP (2009a) Correction of pulmonary arteriovenous malformation using image-based surgical planning. JACC Cardiovasc Imaging 2:1024–1030

Sundareswaran KS, Frakes DH, Fogel MA, Soerensen D, Oshinski JN, Yoganathan AP (2009b) Optimum fuzzy filters for phase-contrast magnetic resonance imaging segmentation. J Magn Reson Imaging 29:155–165

Sundareswaran KS, Haggerty CM, de Zélicourt DA, Dasi LP, Pekkan K, Frakes DH, Powell AJ, Kanter KR, Fogel MA, Yoganathan AP (2012) Visualization of flow structures in Fontan patients using three-dimensional phase contrast magnetic resonance imaging. J Thorac Cardiovasc Surg 143:1108–1116